



direct topochemical polymerizations,<sup>30</sup> and enhance electronic communication within noncovalent assemblies.<sup>31–34</sup> Here, we explore their ability to impart additional strength to macrocycle assemblies by assembling two pentagonal macrocycles derived from diamine, **1**, condensed with either terephthalaldehyde (**2**) or its perfluorinated analogue (**3**, Fig. 1). Both macrocycles separately assemble into high-aspect ratio nanotubes upon protonation, as evident by atomic force microscopy (AFM) and synchrotron *in solvo* X-ray diffraction (XRD). However, upon protonation, a 1 : 1 stoichiometric mixture of the macrocycles assembles into nanotubes with enhanced crystallinity due to AP interactions that reinforce the structure. Touch-spinning fibers from solutions of each nanotube type provided insight into the effects of AP interactions on the nanotube's mechanical properties. Nanotube-loaded (99 wt%) fibers supported by AP interactions exhibited Young's moduli of 2.1 GPa, a 93% increase relative to those of nanotube fibers bearing solely aromatic or perfluoroaromatic residues, 1.09 and 0.49 GPa, respectively. These findings demonstrate that AP interactions are a powerful tool in constructing robust nanomaterials and represent the first example of directly comparing the mechanical effects of AP interactions on supramolecular assemblies to analogous non-AP assembled systems. More broadly, this work highlights how coupled synthetic design and nanoscale assembly can be used to construct materials with useful properties.

## Results and discussion

**NT1** and **NT2** are each synthesized in a single step by condensing the 2,4,6-triphenylpyridine-based diamine (**1**) with either terephthalaldehyde (**2**) or 2,3,5,6-tetrafluoroterephthalaldehyde (**3**) in the presence of  $\text{CF}_3\text{CO}_2\text{H}$  (0.5

equiv. relative to **1**) as a catalyst. In addition to catalyzing imine formation and exchange, the acid protonates the pyridine group of **1** and its condensed products. Electrostatic interactions between co-assembled cationic macrocycles and  $\text{CF}_3\text{CO}_2^-$  drives assembly into nanotubes, which are further stabilized by secondary solvophobic interactions from the aliphatic side chains. This one pot synthesis results in high yields of macrocycle formation relative to other potential imine-linked products.<sup>35,36</sup> Neutral, monomeric [5 + 5] imine-linked macrocycles (**MC1** and **MC2**, respectively) are isolated in high yields (81% each) from these gelled reaction mixtures after neutralization with triethylamine, isolation by centrifugation, and subsequent washing with solvents in which the macrocycles are not soluble (see ESI† for detailed synthesis and purification procedures).<sup>21</sup> The neutral macrocycles were then characterized by matrix-assisted laser desorption/ionization time of flight mass spectrometry (MALDI-TOF MS), size exclusion chromatography (SEC), and  $^1\text{H}$  NMR spectroscopy. SEC of both macrocycles showed a single narrow elution band consistent with the formation of single macrocyclic products (Fig. 2A). MALDI-TOF MS exclusively provided the expected  $[\text{M} + \text{H}]^+$  adducts at 2958.23 *m/z* and 3317.87 *m/z* for **MC1** and **MC2**, respectively (Fig. 2B). In both cases, no oligomeric species, which have substantially higher ionization efficiencies than the macrocycles were observed. Both macrocycles exhibited a  $^1\text{H}$  NMR spectrum consisting of well-defined resonances that are consistent with a symmetric macrocycle (Fig. S5 and S6†). **MC1** was soluble in a variety of organic solvents, yielding a  $^1\text{H}$  NMR spectrum with no resonances corresponding to free aldehydes (*ca.* 10 ppm) or amines (*ca.* 5.5 ppm), further validating the macrocyclic structure. The lower solubility of **MC2** required long sonication times to obtain a  $^1\text{H}$  NMR spectrum with

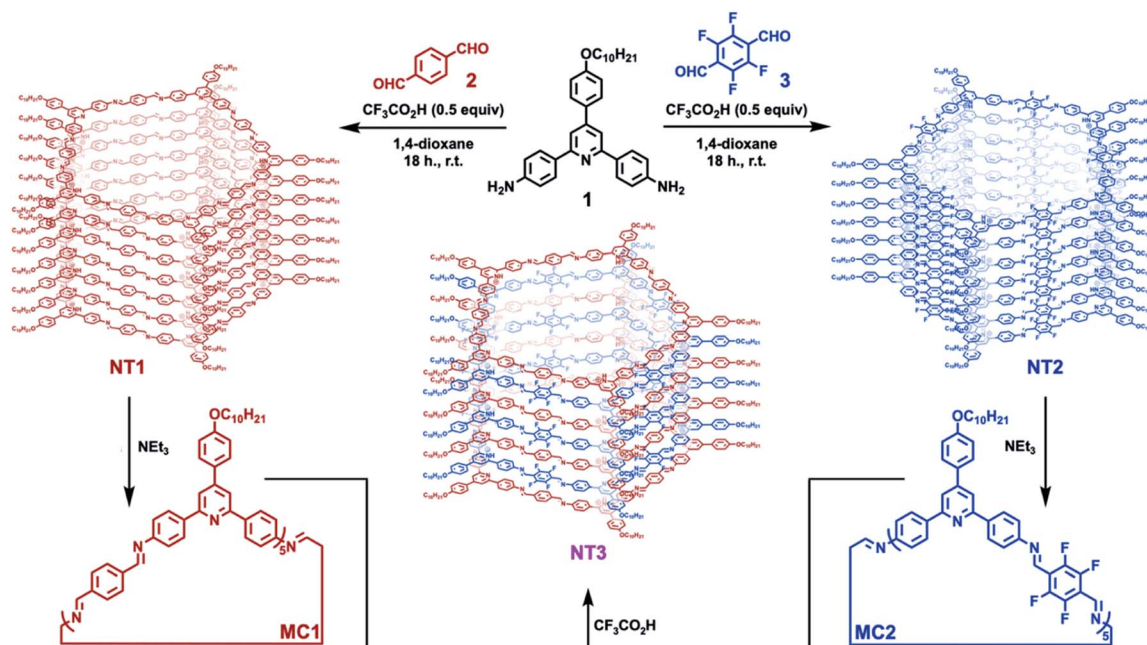


Fig. 1 Synthesis of pentagonal [5 + 5] imine-linked macrocycles and their assembly into the corresponding nanotube, along with an alternating nanotube prepared from a binary mixture of macrocycles.



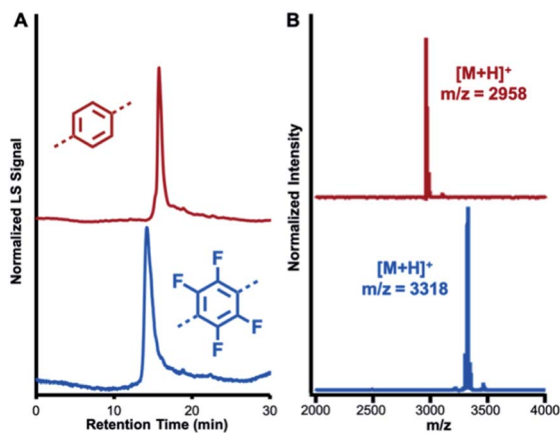


Fig. 2 Characterization of MC1 (red) and MC2 (blue). (A) SEC traces using a multi-angle light scattering (MALS) detector (B) MALDI-TOF MS spectra of MC1 and MC2.

adequate signal-to-noise, and this sample preparation also resulted in the appearance of low-intensity resonances, which we assign as small amounts of ring-opened oligomeric side-products. We attribute the appearance of these oligomers to the conditions needed to fully solvate the macrocycle for NMR spectroscopy because characterization of MC2 by SEC and MALDI-MS prior to sonication did not show evidence of these linear products. However, MALDI-TOF MS performed after sonication did show peaks corresponding to linear oligomers (Fig. S9<sup>†</sup>). Taken together, these data demonstrate that MC1 and MC2 are formed efficiently and isolated in high purity, which enabled further study of their assembly and co-assembly.

Protonation of the pyridine groups within MC1, MC2, and a system prepared from a 1 : 1 mixture of both macrocycles induce their assembly into crystalline nanotubes (NT1, NT2, and NT3, respectively), as evaluated by *in solvo* synchrotron XRD and AFM, Fig. 3. After allowing the macrocyclization reaction to equilibrate for 24 h, the resulting gel was placed into a capillary tube and subjected to synchrotron *in solvo* XRD measurements. The assembly of macrocycles prepared from **1** into nanotubes is characterized by the emergence of a diffraction feature between 0.11 and 0.12 Å<sup>-1</sup>, corresponding to a macrocycle with an internal cavity of *ca.* 3.00 nm. For NT1 this peak is observed at 0.12 Å<sup>-1</sup>, along with the presence of higher order diffraction peaks, indicative of a highly crystalline material. Similarly, NT2 demonstrated a diffraction feature at 0.11 Å<sup>-1</sup>, confirming its assembly into nanotubes of a similar size and shape. NT3 was prepared by suspending purified MC1 and MC2 in 1,4-dioxane and inducing assembly through the addition of CF<sub>3</sub>CO<sub>2</sub>H (1 equiv. per macrocycle). This acid loading ensures that the threshold for assembly is met,<sup>20,21</sup> while being sufficiently low to avoid free CF<sub>3</sub>CO<sub>2</sub>H that impedes nanotube processing by touch-spinning. NT3 exhibits a prominent diffraction feature at 0.12 Å<sup>-1</sup>, indicative of the formation of a crystalline material with similar periodicity as NT1 and NT2. However, the full-width at half max of the <100> and the higher ordering scattering features is significantly decreased in the mixed system relative to either NT1 or NT2, signifying enhanced crystallinity

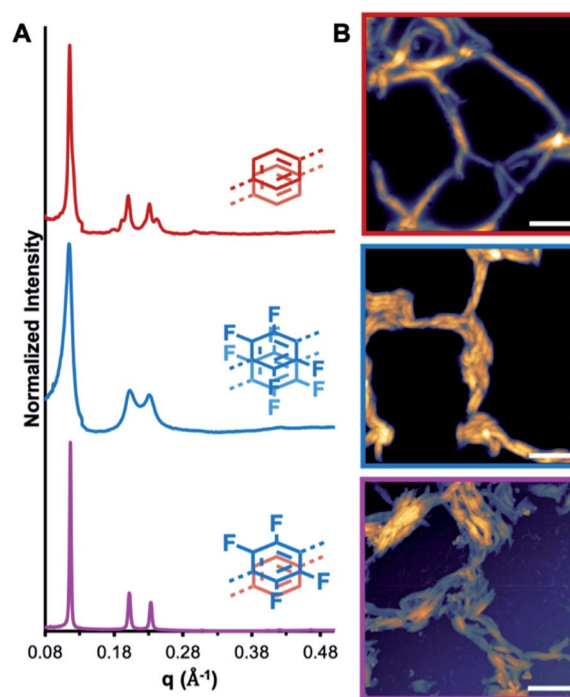


Fig. 3 Characterization of nanotubes prepared through macrocycle assembly. (A) *In solvo* synchrotron XRD patterns of NT1 (red), NT2 (blue), and NT3 (pink). (B) AFM images (2 μm scale bar) of NT1 (red), NT2 (blue), and NT3 (pink).

in the mixed macrocycle system. We attribute the enhanced crystallinity in this system to the formation of AP interactions that are not available to either of the parent systems. While *in solvo* XRD demonstrates macrocycle assembly, AFM of nanotube drop-cast solutions revealed that these assemblies are formed as high-aspect ratio structures with lengths on the order of microns. Aliquots of the mixtures were diluted and drop-cast onto a silicon wafer and imaged by AFM. In the case of NT1, nanotube bundles approximately 50 nm across are observed, while NT2 formed larger, more uniform bundles from nanotubes ranging in diameter from 50 to 500 nm. NT3 is observed as nanotube bundles approximately 500 nm in diameter are comprised of smaller nanotubes. Pyridinium ions are presumed to be the guiding factor in these assembly processes due to the enhanced basicity of the pyridines relative to the imines, and the inability for structurally similar macrocycles lacking pyridine groups to assemble under identical conditions.<sup>35</sup> Taken together, the emergence of strong diffraction signals and direct imaging observations highlight that MC1, MC2, and their mixed system assemble into high-aspect ratio nanotubes under mild conditions, thereby enabling further study into the effects of AP interactions on the mechanical strengths of mixed assemblies.

UV-Vis and fluorescence spectroscopy demonstrate that NT3 exhibit spectral features associated with AP interactions. Macrocycle solutions (5 mM) in 1,4-dioxane were acidified with CF<sub>3</sub>CO<sub>2</sub>H (1 equiv. per macrocycle), diluted to 5 μM, and subjected to UV-Vis and fluorescence spectroscopy. In all cases, acid





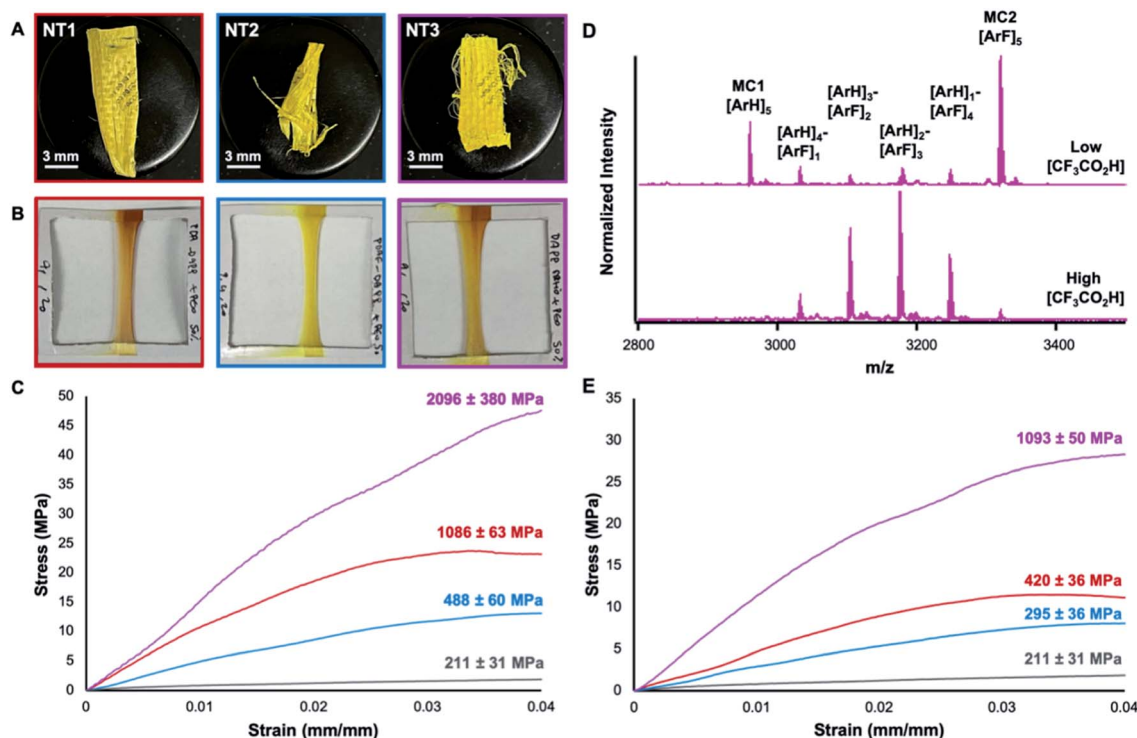


Fig. 4 Mechanical testing of touch-spun nanotube-loaded fibers. (A) Optical images of touch-spun nanotube-loaded fibers. (B) Optical images of mounted fibers before tensile testing. (C) Tensile stress–strain behavior of the touch-spun nanotube fibers formed from low acid loadings and a touch-spun PEO control sample (gray). (D) MALDI-TOF MS spectra of degraded NT3 fibers depicting (top) low degrees of macrocycle scrambling in the presence of low acid concentrations and (bottom) statistical macrocycle scrambling in the presence of large excesses of CF<sub>3</sub>CO<sub>2</sub>H. (E) Tensile stress–strain behavior of the touch-spun nanotube fibers formed from higher acid loadings.

addition resulted in an increase in the emission intensity between 300 and 600 nm ( $\lambda_{\text{ex}} = 340$  nm), which we attribute to a decreased number of non-radiative relaxation pathways in rigid molecular assemblies. The co-assembly of MC1 and MC2 exhibit the hallmarks of AP interactions in its fluorescence signature, specifically a 5-nm blue shift relative to the neutral macrocycle solutions ( $\lambda_{\text{ex}} = 340$  nm) (Fig. S26<sup>†</sup>). The magnitude of this shift is consistent with previous reports on AP interactions that are induced without the formation of charge transfer complexes.<sup>33,37</sup> This shift was not observed in the spectra of NT1 or NT2 over the same period of time, further validating that the observed shift due to AP interactions ( $\lambda_{\text{ex}} = 340$  nm, Fig. S22–S25<sup>†</sup>). Taken together, these data demonstrate that NT3 is supported by additional AP interactions, not accessible in either NT1 or NT2, and inspired studies into how these interactions could impact the mechanical strength of the assemblies.

Touch-spun nanofibers possessing nanotube assemblies demonstrated that AP interactions present in NT3 persist when placed in composite fibers and lead to enhanced mechanical properties relative to fibers possessing nanotubes that lack such interactions. Solutions of MC1, MC2, and a stoichiometric 1 : 1 mixture of MC1 : MC2 in 1,4-dioxane (5 mM) were acidified with CF<sub>3</sub>CO<sub>2</sub>H (1 equiv. per macrocycle) and mixed with 1 wt% of poly(ethylene oxide) (PEO,  $M_n = 4\,000\,000$  g mol<sup>-1</sup>). The addition of PEO increases the viscosity of the nanotube solutions

and affords the fabrication of nanofibers *via* touch spinning (Whiff LLC). In the touch-spinning process, nanotube solutions are pushed through a syringe pump, where droplets released from the tip form a liquid bridge with bars on a nearby rotating disc.<sup>17</sup> As the disc rotates and the polymer is stretched, the solvent evaporates rapidly to form fibers. Cross-sectional scanning electron microscopy (SEM) indicated the high uniformity of the fibers ( $\varnothing = 8.8 \pm 0.6$   $\mu\text{m}$ ,  $14 \pm 1.3$   $\mu\text{m}$ , and  $3.7 \pm 0.3$   $\mu\text{m}$  for NT1, NT2, and NT3, respectively), (Fig. S35–S37<sup>†</sup>). The prepared fibers were then mounted and subjected to uniaxial tensile testing which revealed Young's modulus of  $1086 \pm 63$  MPa (NT1, red) and  $488 \text{ MPa} \pm 60$  (NT2, blue) for assemblies lacking AP interactions. However, when present, AP interactions in touch-spun nanotube fibers resulted in a 93% increase in the Young's modulus (NT3:  $2096 \pm 380$  MPa, pink) (Fig. 4C). The observed increase in the elastic modulus highlights the utility of AP interactions in enhancing the mechanical properties of supramolecular assemblies.

The macrocycles exhibited chemical stability through the assembly and touch-spinning process. After the touch-spinning process, intact, pure MC1 and MC2 were recovered from the nanotubes by dispersing the fibers in triethylamine, leading to deprotonation of the pyridinium moiety and macrocycle disassembly. The insoluble macrocycles were then recovered by centrifugation, and characterized by MALDI-TOF MS. MC1 and MC2 were recovered from NT1 and NT2 and were respectively



observed as the  $[M + H]^+$  adduct at  $m/z$  2959.35 and 3320.23 (Fig. S10–S11†). In samples of NT3, recovered MC1 and MC2 were observed as the corresponding  $[M + H]^+$  adducts at  $m/z$  2959.30 and 3319.04, respectively (Fig. 4D). MALDI-TOF MS of the macrocycles recovered from NT3 also revealed minor peaks corresponding to small amounts of exchange of arene and perfluoroarene groups among MC1 and MC2 during the assembly, touch-spinning and/or recovery process. Given that MC1 and MC2 have similar mass spectrometry ionization efficiencies, these scrambled products are minor and not disruptive of assembly. Nevertheless, we set out to explore this exchange process and its impact on nanotube assembly by intentionally scrambling the macrocycles to a greater extent.

Nanotubes prepared from scrambled macrocycles bearing statistical distributions of 2 and 3 exhibited Young's moduli lower than NT3, but still greater than NT1 or NT2. Intentionally scrambled species were prepared by mixing as-synthesized samples of NT1 and NT2 in a 1 : 1 ratio and equilibrating them with higher concentrations of  $CF_3CO_2H$  for 24 h. Neutralization of the scrambled system and analysis by MALDI-TOF MS demonstrated a statistical scrambling of both dialdehyde monomers, yielding four new macrocycles with varying perfluoro and perhydro subunits (Fig. 4D). Despite this scrambling, fibers touch-spun from the scrambled nanotubes exhibited a Young's modulus of  $1093 \pm 50$  MPa, compared to  $420 \pm 36$  and  $295 \pm 36$  MPa obtained from NT1 and NT2 samples prepared under equally high acid concentrations, respectively (Fig. 4E). We attribute the enhanced mechanical strength in the scrambled species to the formation of many AP interactions even if not every structure can maximize the alternation of its aryl and perfluoroaryl groups. Taken together with the mechanical strengths of pure NT3, these data demonstrate how collective AP interactions are a powerful tool in tuning the mechanical properties of macrocycle assemblies and has resulted in the stiffest nanotubes to date. These findings will spur further research efforts into exploring additional non-covalent interactions to further enhance the mechanical properties of these nanotube assemblies.

## Conclusions

Nanotubes prepared from the co-assembly of macrocycles bearing aromatic and perfluoroaromatic residues exhibit significantly enhanced Young's moduli compared to nanotubes lacking such interactions. A one pot synthesis of NT1 and NT2 occurs through condensation of 1 with either 2 or 3, subsequent deprotonation leads to the isolation of MC1 and MC2. A 50 : 50 mixture of MC1 and MC2 formed a mixed nanotube (NT3) with both arene and perfluoroarene subunits. We demonstrate the dual system's assembly through *in solvo* synchrotron XRD measurements, which demonstrate enhanced crystallinity within NT3, relative to NT1 and NT2. Furthermore, AFM imaging of the mixed system revealed nanotube bundles approximately 500 nm in diameter. Fluorescence spectroscopy suggests AP interactions are present in NT3 through a 5 nm blueshift upon assembly that is not present in either NT1 or NT2. Touch-spinning the assemblies into fibers demonstrates

their processability and also allows for uniaxial tensile testing, which reveals a Young's modulus of 2.096 GPa for NT3, a 93% increase from NT1 (1.086 GPa). This direct comparison of AP and analogous non-AP systems demonstrates how beneficial leveraging secondary interactions such as AP interactions can be in supramolecular assemblies and offers the opportunity to further enhance the nanotubes mechanical strength through orthogonal non-covalent interactions.

## Data availability

All characterization data is available in the ESI.† Raw data sets are available from the corresponding authors.

## Author contributions

Conceptualization: EKR, DA, MJS, AME, MLB, WRD. Investigation: EKR, DA, AK. Methodology: EKR, DA, AK, MJS. Funding acquisition, supervision: MLB, WRD. Writing – original draft, writing – review and editing: all authors.

## Conflicts of interest

The authors declare no competing financial interests.

## Acknowledgements

E. K. R was supported by the Department of Energy (DOE) under grant no. (DE-SC0019356). M. L. B was supported by the National Science Foundation (NSF) under Grant No. (DMR 1507420). M. J. S was supported by the NSF through the Graduate Research Fellowship Program (GRFP) under Grant No. (DGE-1842165). M. J. S. is partially supported by the Ryan Fellowship and the International Institute for Nanotechnology. A. M. E. was supported by the NSF through the GRFP under Grant No. (DGE-1324585). This work made use of the Integrated Molecular Structure Education and Research Center (IMSERC) at Northwestern University, which has received support from the NSF (CHE-1048773), the Soft and Hybrid Nanotechnology Experimental (SHyNE) Resource (NSF; NNCI-1542205), the State of Illinois, and the International Institute for Nanotechnology (IIN). This work also made use of the Scanned Probe Imaging and Development (SPID), and the Electron Probe Instrumentation Center (EPIC), facilities of Northwestern University's Atomic and Nanoscale Characterization Experiment Center (NUANCE), which has received support from the Soft and Hybrid Nanotechnology Experimental (SHyNE) Resource (NSF; ECCS-1542205). This work was also supported by the Northwestern University Keck Biophysics Facility and a Cancer Center Support Grant (NCI CA060553). Parts of this work were performed at the DuPont-Northwestern-Dow Collaborative Access Team (DND-CAT) located at Sector 5 of the Advanced Photon Source (APS) at Argonne National Lab. This research used resources of the Advanced Photon Source and the Center for Nanoscale Materials, both U.S. Department of Energy (DOE) Office of Science User Facilities operated for the DOE Office of



Science by Argonne National Laboratory under Grant No. (DGE-1324585).

## References

- M. Fischer, G. Lieser, A. Rapp, I. Schnell, W. Mamdouh, S. De Feyter, F. C. De Schryver and S. Hoger, *J. Am. Chem. Soc.*, 2004, **126**, 214–222.
- S. Iijima, *Nature*, 1991, **354**, 56–58.
- K. Sato, Y. Itoh and T. Aida, *J. Am. Chem. Soc.*, 2011, **133**, 13767–13769.
- T. Shimizu, W. Ding and N. Kameta, *Chem. Rev.*, 2020, **120**, 2347–2407.
- M. Stepien, B. Donnio and J. L. Sessler, *Angew. Chem., Int. Ed.*, 2007, **46**, 1431–1435.
- J. Zhang and J. S. Moore, *J. Am. Chem. Soc.*, 1994, **116**, 2655–2656.
- N. Kameta, W. Ding and J. Dong, *ACS Omega*, 2017, **2**, 6143–6150.
- N. Kameta, J. Dong and H. Yui, *Small*, 2018, **14**, e1800030.
- A. J. Helsel, A. L. Brown, K. Yamato, W. Feng, L. Yuan, A. J. Clements, S. V. Harding, G. Szabo, Z. Shao and B. Gong, *J. Am. Chem. Soc.*, 2008, **130**, 15784–15785.
- H. Xu, S. Nagasaka, N. Kameta, M. Masuda, T. Ito and D. A. Higgins, *Phys. Chem. Chem. Phys.*, 2016, **18**, 16766–16774.
- H. Xu, S. Nagasaka, N. Kameta, M. Masuda, T. Ito and D. A. Higgins, *Phys. Chem. Chem. Phys.*, 2017, **19**, 20040–20048.
- P. Beker, I. Koren, N. Amdursky, E. Gazit and G. Rosenman, *J. Mater. Sci.*, 2010, **45**, 6374–6378.
- X. Xu, S. Chen, Y. Chen, H. Sun, L. Song, W. He and X. Wang, *Small*, 2016, **12**, 2982–2990.
- Y. Xu, T. Wang, Z. He, A. Zhong, W. Yu, B. Shi and K. Huang, *Polym. Chem.*, 2016, **7**, 7408–7415.
- J. Yang, M. B. Dewal and L. S. Shimizu, *J. Am. Chem. Soc.*, 2006, **128**, 8122–8123.
- D. T. Bong, T. D. Clark, J. R. Granja and M. R. Ghadiri, *Angew. Chem., Int. Ed.*, 2001, **40**, 988–1011.
- S. Dong, B. Zheng, F. Wang and F. Huang, *Acc. Chem. Res.*, 2014, **47**, 1982–1994.
- X. Yan, F. Wang, B. Zheng and F. Huang, *Chem. Soc. Rev.*, 2012, **41**, 6042–6065.
- C. Sun, M. Shen, A. D. Chavez, A. M. Evans, X. Liu, B. Harutyunyan, N. C. Flanders, M. C. Hersam, M. J. Bedzyk, M. Olvera de la Cruz and W. R. Dichtel, *Proc. Natl. Acad. Sci. U.S.A.*, 2018, **115**, 8883–8888.
- M. J. Strauss, D. Asheghali, A. M. Evans, R. L. Li, A. D. Chavez, C. Sun, M. L. Becker and W. R. Dichtel, *Angew. Chem., Int. Ed.*, 2019, **58**, 14708–14714.
- M. J. Strauss, M. Jia, A. M. Evans, I. Castano, R. L. Li, X. Aguilar-Enriquez, E. K. Roesner, J. L. Swartz, A. D. Chavez, A. E. Enciso, J. F. Stoddart, M. Rolandi and W. R. Dichtel, *J. Am. Chem. Soc.*, 2021, **143**(21), 8145–8153.
- L. M. Salonen, M. Ellermann and F. Diederich, *Angew. Chem., Int. Ed.*, 2011, **50**, 4808–4842.
- S. S. Babu, V. K. Praveen, S. Prasanthkumar and A. Ajayaghosh, *Chem. –Eur. J.*, 2008, **14**, 9577–9584.
- K. B. Woody, J. E. Bullock, S. R. Parkin and M. D. Watson, *Macromolecules*, 2007, **40**, 4470–4473.
- H. X. Wu, B. B. Ni, C. Wang, F. Zhai and Y. G. Ma, *Soft Matter*, 2012, **8**, 5486–5492.
- R. Xu, B. Schweizer and H. Frauenrath, *J. Am. Chem. Soc.*, 2008, **130**, 11437–11445.
- C. Y. Dai, P. Nguyen, T. B. Marder, A. J. Scott, W. Clegg and C. Viney, *Chem. Commun.*, 1999, 2493–2494, DOI: 10.1039/a906199a.
- M. Weck, A. R. Dunn, K. Matsumoto, G. W. Coates, E. B. Lobkovsky and R. H. Grubbs, *Angew. Chem., Int. Ed.*, 1999, **38**, 2741–2745.
- R. E. Yardley, J. A. Paquette, H. Taing, H. M. Gaebler, S. H. Eichhorn, I. P. Hamilton and K. E. Maly, *Org. Lett.*, 2019, **21**, 10102–10105.
- A. F. Kilbinger and R. H. Grubbs, *Angew. Chem., Int. Ed.*, 2002, **41**, 1563–1566.
- K. P. Castro, E. V. Bukovsky, I. V. Kuvychko, N. J. DeWeerd, Y. S. Chen, S. H. M. Deng, X. B. Wang, A. A. Popov, S. H. Strauss and O. V. Boltalina, *Chem. –Eur. J.*, 2019, **25**, 13547–13565.
- Y. Q. Sun, Y. L. Lei, L. S. Liao and W. P. Hu, *Angew. Chem., Int. Ed.*, 2017, **56**, 10352–10356.
- H. W. Zhang, J. L. Han, X. Jin and P. F. Duan, *Angew. Chem., Int. Ed.*, 2021, **60**, 4575–4580.
- X. H. Zhou, J. D. Luo, S. Huang, T. D. Kim, Z. W. Shi, Y. J. Cheng, S. H. Jang, D. B. Knorr, R. M. Overney and A. K. Y. Jen, *Adv. Mater.*, 2009, **21**, 1976–1981.
- A. D. Chavez, A. M. Evans, N. C. Flanders, R. P. Bisbey, E. Vitaku, L. X. Chen and W. R. Dichtel, *Chem. –Eur. J.*, 2018, **24**, 3989–3993.
- M. J. Strauss, A. M. Evans, I. Castano, R. L. Li and W. R. Dichtel, *Chem. Sci.*, 2020, **11**, 1957–1963.
- A. Mandal, A. Choudhury, P. K. Iyer and P. Mal, *J. Phys. Chem. C*, 2019, **123**, 18198–18206.

